Turkish Journal of Electrical Engineering & Computer Sciences

http://journals.tubitak.gov.tr/elektrik/

Research Article

Turk J Elec Eng & Comp Sci
(2021) 29: 673 – 686

doi:10.3906/elk-2002-91

Long term stability of 1.3 GHz high power RF amplifier

Özlem KARSLI[1,*], **Evrim ÇOLAK**[1,2]

[1]Institute of Accelerator Technologies, Ankara University, Ankara, Turkey

[2]Electrical and Electronics Engineering Department, Faculty of Engineering, Ankara University, Ankara, Turkey

Received: 14.02.2020 • **Accepted/Published Online:** 12.10.2020 • **Final Version:** 30.03.2021

Abstract: Turkish accelerator and radiation laboratory (TARLA) is an accelerator based oscillator mode free electron laser (FEL) facility under construction. The acceleration beamline includes a fundamental buncher (FB) in order to confine the electron beam into a compressed bunch. In this study, we demonstrate the commissioning tests of 500 W RF amplifier powering FB and present the phase stability dependence on the pressure and temperature of the water cooling line under long time run conditions. As the disturbing effects break down the synchronization between the particle and RF power during acceleration, the reasons disquieting the stability of the RF amplifier are investigated. One reason which causes disturbance in the stability is the variation in the phase of the output power. Phase variation of the output power of the RF amplifier which was measured as $\sim$10 deg/$^\circ$C in average initially, which was beyond permitted variation levels by the controller electronics, namely the low level RF system (LLRF), is decreased to less than $\sim$0.45 deg/$^\circ$C by incorporating a phase shifter. In addition, this phase variation reduction is accompanied with a reflected power at the output of the RF amplifier decline from 4.3 W (36.33 dBm) down to 3 mW (4.7 dBm) by utilizing a circulator, which is also important and desirable in terms of protection of the electronics in the long term run. As ensuring phase stability in the output power is very important, this work may serve as a guide since the documentation regarding the output power dependence of the water cooling line for long term run is very limited.

Key words: High power, long term stability, operation performance, RF, high frequency

1. Introduction

Turkish accelerator and radiation laboratory (TARLA) [1, 2] is under construction to realize a linear accelerator that will deliver a 1 mA continuous (cw) electron beam to produce free electron laser (FEL) radiation. Additionally, we pay attention to generation of bremsstrahlung radiation from deceleration of electron beam in matter which will serve as a photon source in a wide range of application fields including nuclear physics [3].

TARLA accelerator beamline is composed of an injector line in low-energy covering subharmonic (SHB) and fundamental (FB) buncher cavities together with a main accelerator line in high-energy including two superconducting (SC) cryomodules. Thermionic gun releases electrons with 250 keV of energy in $\sim$600 ps bunch lengths at 13 MHz operation frequency. SHB and FB are used to focus the electron beam longitudinally by velocity modulation, i.e. energy modulation, to maintain the bunch length and to match the beam into the entrance of the SC linear accelerator (linac). SHB and FB are normal conducting accelerating cavities which operate at 260 MHz and 1.3 GHz, respectively. Thermionic injector line contributes to ensure the beam quality

*Correspondence: okarsli@ankara.edu.tr

before electrons enter the main accelerators, i.e. SC cryomodules. Due to this compression process, these cavities are also called as bunch compressors. When the installation of the injector is completed, the TARLA injector line will deliver electrons with bunch length of ∼0.4–6 ps at the operation frequency of 1.3 GHz [4, 5].

After the injector, there are two SC cryomodules each including two thermally shielded SC TESLA-type [6] radio frequency (RF) cavities which are connected to cryogenic distribution lines to be placed in the TARLA accelerator beamline. These SC cryomodules will accelerate the electron beam within 5–40 MeV energy range. The generated heat load will be cooled by TARLA Helium Cooling System, i.e. cryogenics, which has a capacity of 210 W at 1.8 K.

The SC technology comes with the advantage of very flexible operation with the whole duty cycle (continuous wave, cw, operation), which makes it especially attractive for the use of electron beam interacting with the periodic magnetic fields through the undulator and the radiation field in optical cavity [7]. In this context, TARLA will produce an infrared (IR) FEL within the wavelength range of 5-350 μm and a bremsstrahlung radiation in the energy range of 5–30 MeV at an average electron beam current of 1 mA [8]. According to the concept of becoming a user facility, TARLA is presently preparing a five-laboratory area in clean room standards for FEL experiments.

The phase drift on RF voltage (power signal) powering the accelerating RF cavities directly affects the beam quality parameters, such as emittance, beam energy spread, diffusion of beam transport and phase shift between the beam and RF voltage [4]. Irregular changes in amplitude and phase of RF signal at the output of the RF amplifier can occur due to different reasons such as amplifier gain variation, phase drift of components, etc. This affects the stability of RF field and cause reduced energy gain of particles. The long term stability is defined as the constant phase and gain drift under some fixed threshold level for RF amplifiers. These parameters are crucial for the uninterrupted long time steady state operation, and should not be disturbed by any environmental change. Therefore, significant consideration should be given to correct the phase variation. For this purpose, in this study the phase drift and amplitude variations of 500 W RF power amplifier powering FB have been measured during long time operation. The long time stability tests are performed in the scope of commissioning works of the injector line. Measurements cover the phase and magnitude of the scattering parameters (S-parameters) for the 500 W RF amplifier. These measurements enable us to observe the phase drift and amplitude variations of the amplifier. During the measurements, temperature variations and pressure fluctuations of the cooling water of the amplifiers are also monitored to be processed and compared with the S-parameter measurements. The considered phase drift is corrected by an improved circuit, enabling steady state operation.

2. RF structure of TARLA

High power RF (HPRF) system has six RF stations including solid state amplifiers, waveguide and coaxial distribution systems, interlock system and other auxiliaries in racks to drive RF power to the accelerator sections in the TARLA. The injector is served by two RF stations for powering SHB and FB while main accelerators have four RF stations, two of which provide RF power for each SC cryomodules. The HPRF structure of TARLA is depicted in Figure 1.

The low level radio frequency (LLRF) control of the TARLA accelerator is crucial for the operation of the accelerator, as the system will set and maintain stable acceleration voltage (defining the amplitude of RF power) and phase of the high-precision calibrated vector sum of individual RF stations for synchronization. It is based on Micro TCA (MTCA.4) technology and is developed by DESY [9]. The LLRF system which is used

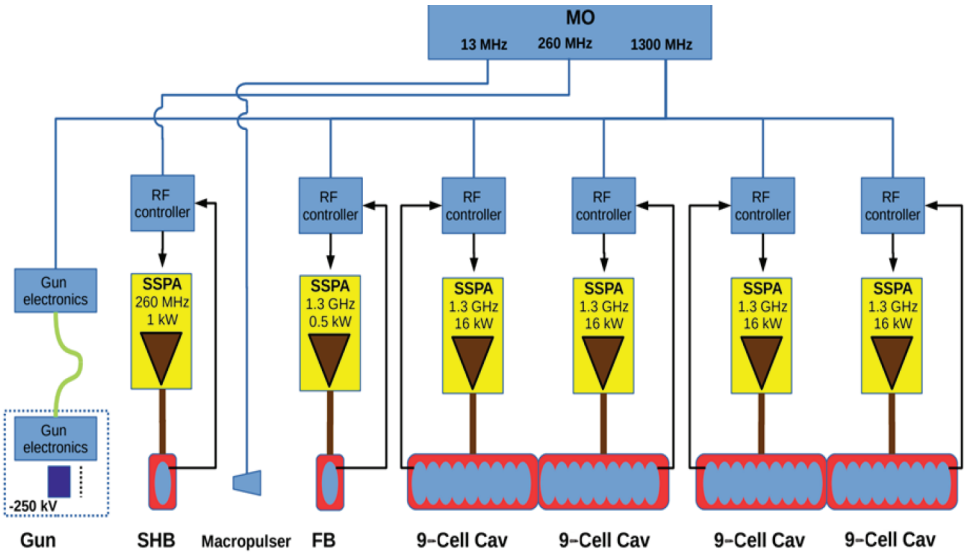

Figure 1. Layout of TARLA HPRF structure [4].

to calibrate signals, will provide a high stable RF reference throughout the accelerator. A master oscillator will provide a highly stable RF reference signal for the LLRF controller. The TARLA LLRF will guarantee an overall field stability variation less than 0.09% in amplitude and phase jitters at the FB. However, in order to ensure the stability, a certain degree of phase adjustment should be performed on the system initially. The correction parameters of TARLA LLRF system is shown in Table 1.

Table 1. The expected regulation levels of TARLA LLRF system [10].

System		Jitter (rms)	Drift (peak-peak)
260 MHz SHB	Amplitude [%]	0.2	0.5
260 MHz SHB	Phase [deg]	0.15	0.2
1300 MHz FB	Amplitude [%]	0.08	0.2
1300 MHz FB	Phase [deg]	0.08	0.1
1300 MHz SC modules	Amplitude [%]	0.05	0.1
1300 MHz SC modules	Phase [deg]	0.04	0.1

The LLRF system will drive all solid state amplifiers of the facility. It will regulate the six RF stations of main acceleration section consisting of two SC cryomodules, i.e. four RF cavities, and injector section including two bunch compressors (SHB and FB), i.e. normal conducting longitudinally compressing structures. Two injector RF stations power the SHB and FB with 1500 W and 500 W solid state RF amplifiers, respectively. There will be a longitudinal feedback system within the LLRF control loop.

Solid state RF power amplifiers are specified to feed the bunch compressors at TARLA. Table 2 lists the basic technical specifications of 500 W RF amplifier to power the 1.3 GHz FB. The parameters listed in Table 2 are in accordance with the beam dynamics computation [4] and the qualifications are compatible with the FB. The efficiency and linearity are the most critical parameters of the specification. Output power of $\sim$ 400 W has been acknowledged by taking the bunch length to be delivered to FB, the heat load capacity of the FB antenna

Table 2. The main parameters of 500 W RF amplifier.

Parameter	RF Amplifier	Unit
Amplifier	Class AB push-pull	
Frequency range	1300 ± 5	MHz
CW & pulsed output power	400@ 1 dB compression	W
Linear gain	≥57	dB
Output harmonics (2nd and 3rd order)	<–45	dBc
Phase drift coefficient (typical)	0.35	deg./C
Gain drift coefficient (typical)	1.2	%/C
Efficiency at 500 W output (typical)	> 45	%
Output phase change from min. to max. power (max.)	±10	deg.
Rise-fall time	< 60	ns
Pulse repetition rate	1-CW	Hz
Pulse length	10-CW	μs

and the cooling capacity of the FB into consideration. The frequency and the bandwidth of the amplifier should be equal to those of the FB. Rise and fall times at the order of nanoseconds provide more effective interaction between the beam and RF power due to the early stabilization. The device was manufactured by SigmaPhi[1] with a spare unit.

3. Performance and stability tests

Theoretical background regarding the affects of phase difference between the particle and RF power is explained clearly in [11]. A moving particle in an RF cavity comes across with the RF field phase. The beam emittance depending on the phase difference and the energy gain causes the beam deviation during the transport line, resulting in an emittance growth and energy spread [11].

Figure 2 shows the block diagram of the measurement setup. S-parameters of the output signal is measured by an Anritsu MS4640A VectorStar^{TM}[2] vector network analyzer (VNA). While Port 1 of VNA excites the RF amplifier, Port 2 samples the transmitted power. S-parameters of the output signal of the RF amplifier reveal the amplitude and phase of the reflected or transmitted power. The data are collected by a personal computer which runs a home-written test routine coded in National Instruments (NI) LabVIEW^{TM} Software[3]. The picture of the experimental setup and the interface of the software are illustrated in Figure 3. The flow diagram of LabVIEW^{TM} code written to control the VNA and to carry out the measurement is given in Figure 4. The test software while providing with the control of VNA, is also used to set the measurement parameters like sampling period, number of samples and the data acquisition method. S-parameters (S_{11}, S_{21}, etc.) are periodically logged throughout the whole experiment. Test interface allows us to follow the instantaneous plots of the measured quantity. The raw data are recorded as a text file and named automatically by the software to indicate the sample number. TARLA has a SCADA system to track the temperature and

[1]SigmaPhi Accelerator Technologies [online]. Website https://www.sigmaphi.fr/ [accessed 07 December 2018].
[2]Anritsu [online]. Website https://www.anritsu.com/en-US/ [accessed 13 December 2018].
[3]National Instruments. LABVIEW [online]. Website http://www.ni.com/en-tr/shop/labview/labview-details.html [accessed 22 March 2019].

the pressure variations of water cooling system. The temperature and pressure data are also logged in weekly periods by the system during the measurement.

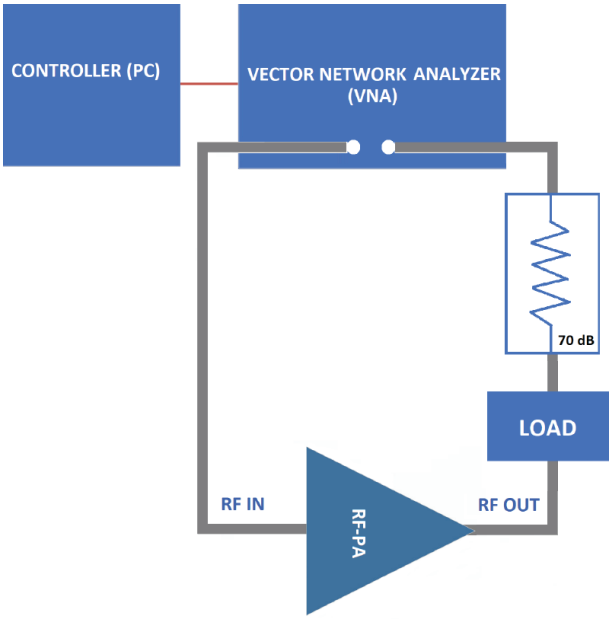

Figure 2. Block diagram of the test setup.

Figure 3. The experimental setup.

Upon completing the measurement, the acquired data are analyzed by MATLAB^{TM} software[4]. A script home-written in MATLAB^{TM} is used to plot the S-parameters, temperature and pressure values of the water cooling system as a function of time, which enables the analysis of the fluctuations of S-parameters graphically. Obtained graphs are shown in Figures 5 and 6.

[4]MathWorks Inc. MATLAB [online]. Website https://www.mathworks.com/products/matlab.html [accessed 22 March 2019].

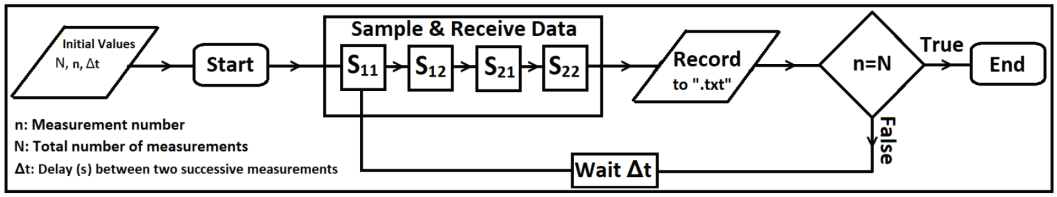

Figure 4. The flow diagram of the LabVIEW^{TM} code which is used to control the system.

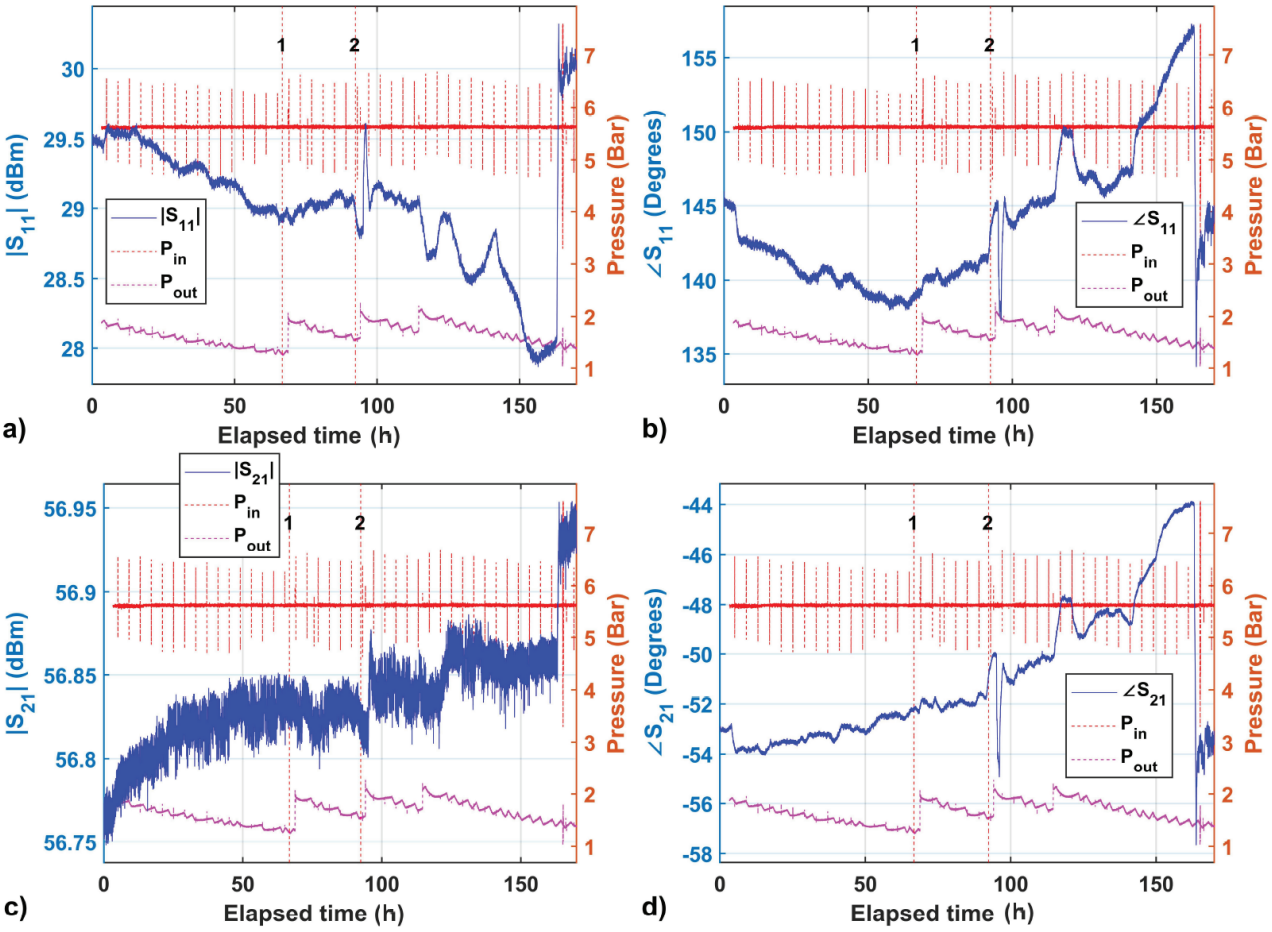

Figure 5. a) Magnitude of reflection coefficient ($|S_{11}|$), b) phase of reflection coefficient ($\angle S_{11}$), c) magnitude of transmission coefficient ($|S_{21}|$), and d) phase of transmission coefficient ($\angle S_{21}$) measurements together with the pressure of water cooling line (right hand side axis) as a function of elapsed time in the experiment.

The amplifier has a protective interlock state against the excessive conditions of power, overheat, low/over flow of water cooling system, etc. During the operation, the heating of VNA also causes interlock due to the fluctuation of the input signal. That is the reason why a relatively low value, which is –0.5 dBm instead of 0 dBm, is applied to the amplifier. This fixing yields $\sim$ 419 W output power from RF amplifier. Another reason for the selection of $\sim$ 419 W as the output power is that approximately this amount of power will be applied to the FB during the routine operation. The reflected power at the output of the RF amplifier is measured as $\sim$

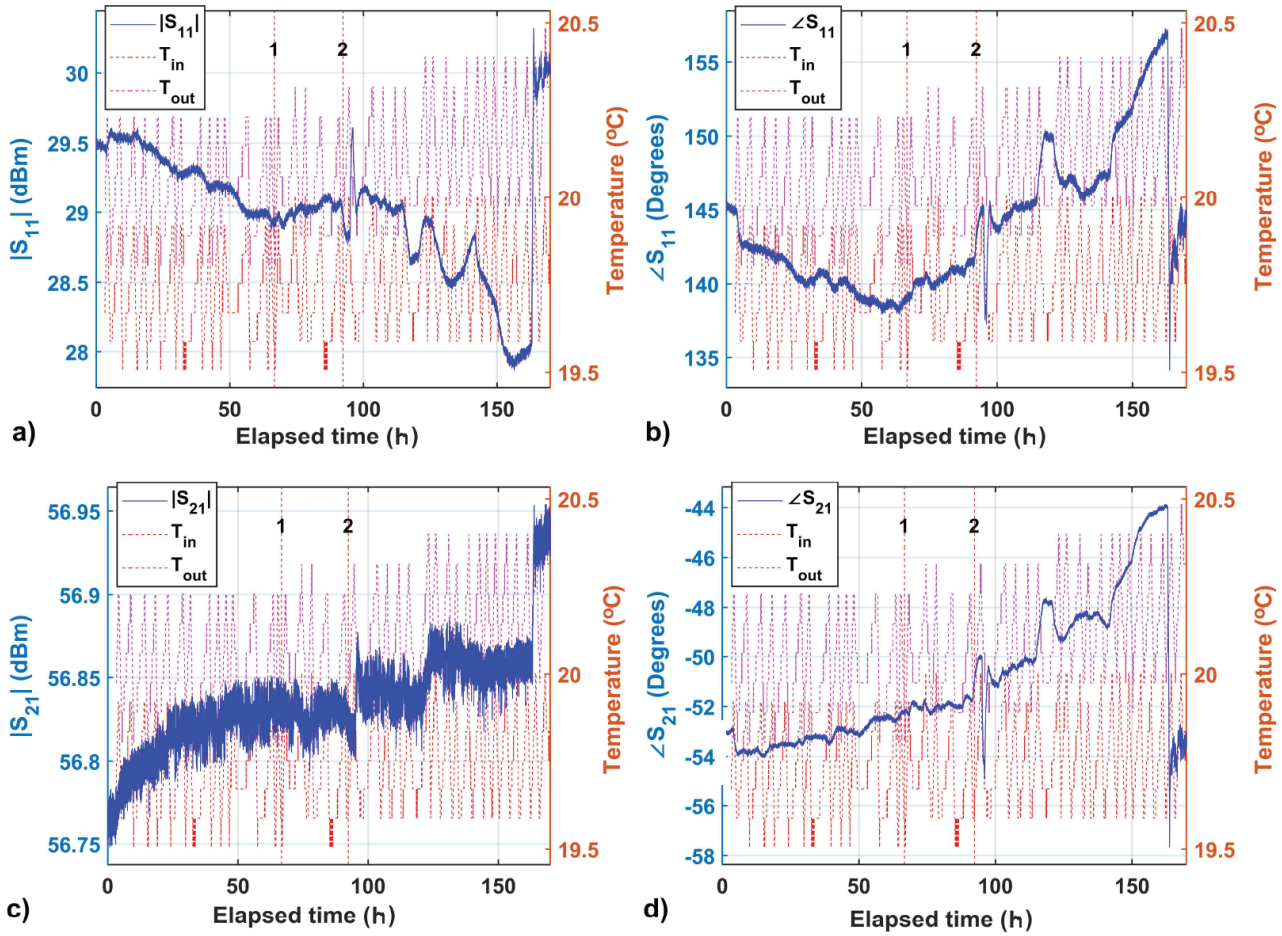

Figure 6. a) Magnitude of reflection coefficient ($|S_{11}|$), b) phase of reflection coefficient ($\angle S_{11}$), c) magnitude of transmission coefficient ($|S_{21}|$), and d) phase of transmission coefficient ($\angle S_{21}$) measurements together with the temperature variation (right hand side axis) as a function of elapsed time in the experiment.

4.3 W ($\sim$ 36.33 dBm) in this composition. The reflection is caused by the connection points (heating, leakage, etc.) and the bending of high power coaxial RF cable.

Figure 5 depicts the phase and magnitude variations in the S-parameters together with the pressure variations of the water cooling system throughout the experiment which is performed at the operation frequency of 1.3 GHz with 500 W amplifier. In the same way, Figure 6 illustrates the phase and magnitude variation of the S-parameters together with the temperature variations of the water cooling system. Blue lines on the graphs show the measured S_{11} or S_{21}, whereas the orange (pink) color is the input and output pressure (temperature) values of the water cooling system. The vertical dashed lines indicate the time instants that the water cooling line experiences external interference (maintenance, commissioning of another equipment utilizing the same cooling line etc.) during the measurements, which would yield instantaneous pressure and temperature variation.

One can understand from Figures 5c and 5d, i.e. S_{21} magnitude and phase graphs, respectively, that the pressure fluctuation level of six bars in the water cooling line is observed to be ineffective on S-parameter stability of the 1.3 GHz amplifier. This is in contrast to the case of the experiment which was carried out with

a distinct amplifier running at 260 MHz [11]. In Ref. [11], it is seen that with the utilization of a distinct 260 MHz RF amplifier, the pressure fluctuation in the water cooling system contributes to the phase variation in the transmitted power. In the literature, to the best of authors' knowledge, no research has been reported such an effect on phase stability of the power transmitted by RF amplifier due to the pressure fluctuations in water cooling system.

It has been reported in Ref. [12] that the circumstantial disruptions, such as electrical noise [13], temperature alteration, disturbance and vibration can potentially degrade the performance of such highly adjustable resonators when they are deployed in the field. Vibration modes are inversely proportional to the square of the frequency. Based on this information, it is concluded that unlike 1300 MHz, 260 MHz may be vulnarable to the effect of upper harmonics of the mechanical vibration modes of water cooling line. Since 1300 MHz is a reasonably high frequency and considering the suppression in the upper harmonics of mechanical vibration modes in comparison to those in the lower frequencies, it is predictable not to observe any correlation between the pressure fluctuations of water cooling line and the transmitted power, S_{21}, in case of 1300 MHz amplifier.

The input signal level of the RF amplifier is –0.5 dBm and the attenuation factors for the output power and reflected power are 70 dB and 50 dB, respectively, in the experiment. The attenuated output power of the amplifier should be ~ -13.75 dBm since S_{21} which is the ratio of output power to the input power is measured as ~ -13.25 dB [–13.75 dBm–(–0.5 dBm)] using the VNA. Taking the attenuation into account, actual output power of the amplifier and the actual S_{21} turn out to be ~ 56.25 dBm (–13.75 + 70) and ~ 56.75 dBm [56.25–(–0.5)], respectively as seen in Figures 5c and 6c. The output power findings of the VNA is verified by utilizing a R&S®NRP2 model power meter[5]. The reading value is found as 419 W ~ 56.22 dBm which corresponds to S_{21} value of ~ 56.72 dBm [56.22 dBm–(–0.5 dBm)].

Stability of the amplifier is another issue to be verified. Specifically, unconditional stability for active two-port networks in a circuit has been widely discussed in literature [14, 15]. Using the measured S-parameters, the stability conditions are examined based on geometrically derived stability parameters including Rollet stability factor (K), source (μ_{source}) and load (μ_{load}) stability factors in addition to other stability parameters and conditions which are given in [15] as follows:

$$K = \frac{1 - |S_{11}|^2 - |S_{22}|^2 + |\Delta|^2}{2|S_{12}S_{21}|} \geq 1 \tag{1}$$

$$\Delta = |S_{11}S_{22} - S_{21}S_{12}| < 1 \tag{2}$$

$$B_1 = 1 + |S_{11}|^2 - |S_{22}|^2 - |\Delta|^2 > 0 \tag{3}$$

$$B_2 = 1 + |S_{22}|^2 - |S_{11}|^2 - |\Delta|^2 > 0 \tag{4}$$

$$\mu_{source} = \frac{1 - |S_{11}|^2}{|S_{22} - \Delta(S_{11}^*)| + |S_{21}S_{12}|} \geq 1 \tag{5}$$

$$\mu_{load} = \frac{1 - |S_{22}|^2}{|S_{11} - \Delta(S_{22}^*)| + |S_{21}S_{12}|} \geq 1 \tag{6}$$

[5]Rohde & Schwarz [online]. Website https://www.rohde-schwarz.com/ph/product/nrp2 [accessed 18 December 2019].

The conditions $\mu_{source} \geq 1$ and $\mu_{load} \geq 1$ are the sufficient conditions for unconditional stability as stated in Ref. [15]. Since the satisfaction of these two conditions also implies $K \geq 1$, $\Delta < 1$, $B_1 > 0$ and $B_2 > 0$, satisfaction of all necessary and sufficient conditions in terms of other stability parameters for unconditional stability is already ensured (i.e. $K \geq 1$ and satisfaction of either one of the following: $\Delta < 1$, $B_1 > 0$ and $B_2 > 0$). It is seen in Figure 7 that μ_{source} and μ_{load} are both greater than unity in the frequency range from 1.29 GHz to 1.31 GHz. Thus, under the light of the above discussion, it is concluded that the recent amplifier system is unconditionally stable as $\mu_{source} \geq 1$ and $\mu_{load} \geq 1$ are satisfied in the defined operation frequency range. Considering 220 samples of S-parameters taken in a 3.7-h-long experiment, the calculated stability parameters μ_{source} and μ_{load} are plotted in the corresponding graphs for each sample which are taken at different sampling time instants. The cumulative series of plots form a narrow band with maximum standard deviation value of 2.79 and 1.80 for μ_{source} and μ_{load}, respectively, in the given frequency range. This narrow band of plots indicate that stability parameters and as a result S-parameters do not change abruptly in long duration of operation. Another remark is the following: seemingly narrow frequency range is in fact sufficient as the actual operation frequency will be 1.30 GHz and will be strongly controlled with a LLRF feedback system.

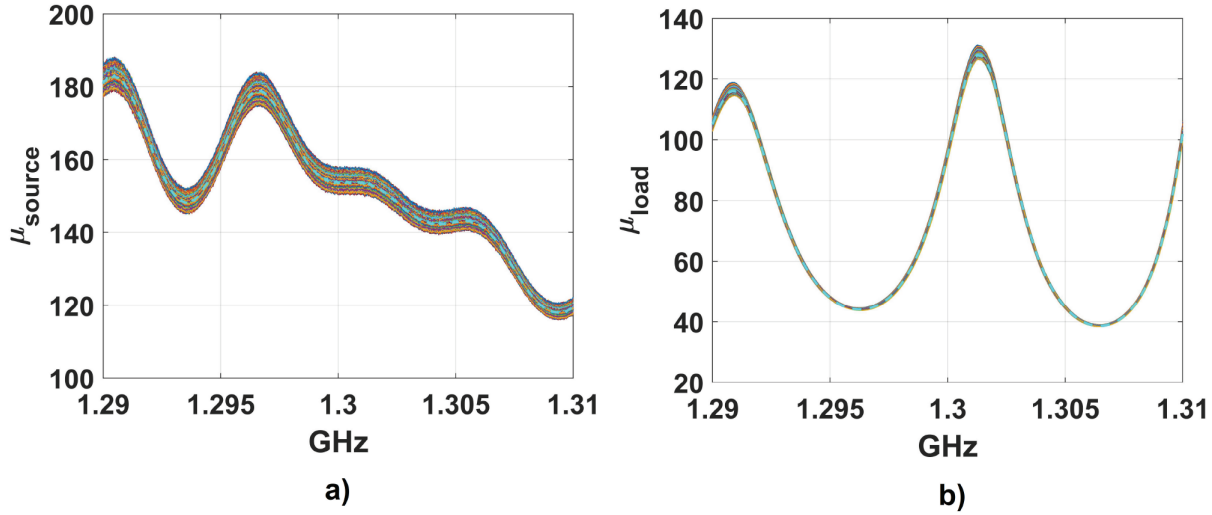

Figure 7. a) μ_{source} based on the experimental S-parameters as a function of frequency, b) μ_{load} based on the experimental S-parameters as a function of frequency. Calculation of μ_{source} and μ_{load} are repeated for 220 samples which are taken approximately in 3.7 h. Each calculation is plotted in the corresponding graph to demonstrate time evolution of the stability parameters. The mean value for μ_{source} and μ_{load} are calculated at each frequency and are plotted in the corresponding graph (dashed turquoise).

Using the experimental S-parameters, Eq. (1) through Eq. (4) are also satisfied in the operational frequency range (not plotted in this paper). As an observation to be mentioned, K attains very high values as high as 10^{15} in form of very narrow spikes while minimum value of K is 8.9×10^{8}, still larger than unity. Thus, Eq. (1) is still satisfied throughout the operation range. Nevertheless, due to the fact that Eq. (1) involves $|S_{12}|$ in the denominator while $|S_{12}|$ has an amplitude distribution very close to 0 in the operation range, spikes occur in K, numerically. This situation is again acceptable and does not disturb the unconditional stability (together with the satisfaction of Eq. (2) through Eq. (4)). Because, in the normal operation $|S_{12}|$ which shows the amount of power flow from Port 2 to Port 1 (i.e. the power flow from load side towards the amplifier)

is expected to be as low as possible, ideally zero. In conclusion, it has been shown by the examination of the stability parameters that the amplifier under test is unconditionally stable and does not have any practical impact on the phase drift in the transmitted power.

This study aims to implement a method to reduce the phase fluctuation and keep it constant under a threshold level to achieve effective transfer of power to the particle in FB. For this purpose, we have incorporated a manual phase shifter and a circulator in the experimental setup. The phase shifter is a passive device that attenuates the signal as a part of operation and the circulator is used to protect the amplifier from the reflected signal which may damage the feeding electronics. Figure 8 shows the block diagram of the improved circuit.

To observe the phase fluctuations in the new setup, the RF amplifier is tested in a separate 20-h run. Figure 9 depicts phase of the transmission coefficient ($\angle\ S_{21}$) for the cases without (Figure 9a, which is zoomed portion from Figure 6d) and with (Figure 9b) phase shifter. Both two graphs are presented comparatively to show the effect of the phase shifter. It is observed that the standard deviation of $\angle\ S_{21}$ is 0.208 in the circuit without phase shifter (Figure 9a). On the other hand, after the use of phase shifter (Figure 9b), a strong correlation between $\angle\ S_{21}$ and temperature becomes evident. Omitting the early hours after the start of amplification, time slot between hour 15 and hour 20 is considered where the amplified signal becomes more stable (marked with a green colored box in Figure 9b). During routine operation of the facility (full load) where all of the chillers (which are used for cooling) and the loads (which generate heat) are functional, variation in the temperature of the water in the cooling system will be negligible. Consequently, a normalization procedure is applied as follows: Values of $\angle\ S_{21}$ in the mentioned time slot are divided by the corresponding water temperature to eliminate the effect of water temperature on $\angle\ S_{21}$. Then, the standard deviation in the normalized $\angle\ S_{21}$ values (which form almost a horizontal line after normalization - not shown here) is calculated as 0.054. Moreover, incorporation of the phase shifter yields a decreased reflection level of 3 mW ($\sim$ 4.7 dBm) which is measured at the output of the power amplifier by using a directional coupler. As a result, amplitude of ripple and variation in the $\angle\ S_{21}$ are reduced, which is critical for the acceleration of charged particles.

Amplitude and phase modulation (AM/PM) can serve for characterization of the power amplifier to identify the phase distortion [16]. Understanding the physical distortion generation mechanisms is significant for linearity during the design of the power amplifiers [17]. We tested the AM/PM characteristics of the RF amplifier by the same set-up which is shown in Figure 8. Output power and the output phase characteristics of the RF amplifier under test are illustrated in Figures 10a and 10b, respectively [16]. It is seen that AM/PM characteristics is typical both in terms of output power amplitude and output phase [16–18]. Diverging from the linear model is evident especially for the input power levels to the right of the input level marked with A^* in Figure 10a which corresponds to 1 dB compression at the output power. A gradual decrease in the output phase which is slower for lower input levels while steeper for higher input levels is also observed, as seen in Figure 10b. The rest of the correction to satisfy the predefined overall system specifications, i.e. further reduction of the phase variation to the specified limits will be performed by TARLA LLRF system (see Table 1) when the overall system becomes fully functional.

4. Conclusion

Recently, the solid state technology applications in RF frequency range have attracted strong interest of the research community for particle accelerator applications. The efforts proceed for better efficiency and output power at component level. However, we still need to improve the reliability and system efficiency which can be

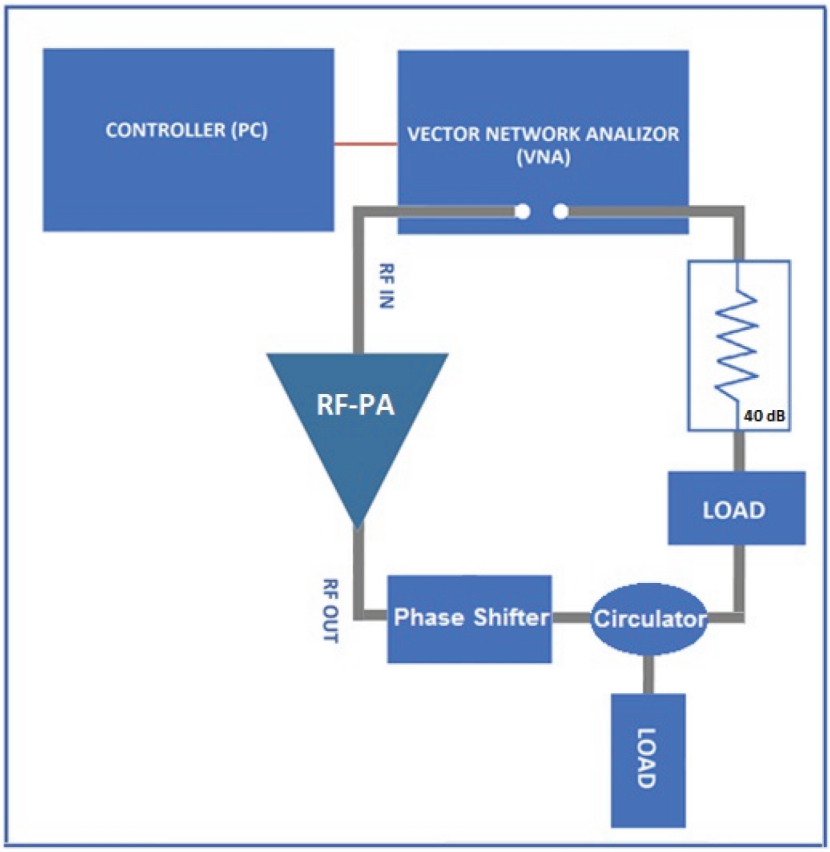

Figure 8. The block diagram of the improved circuit.

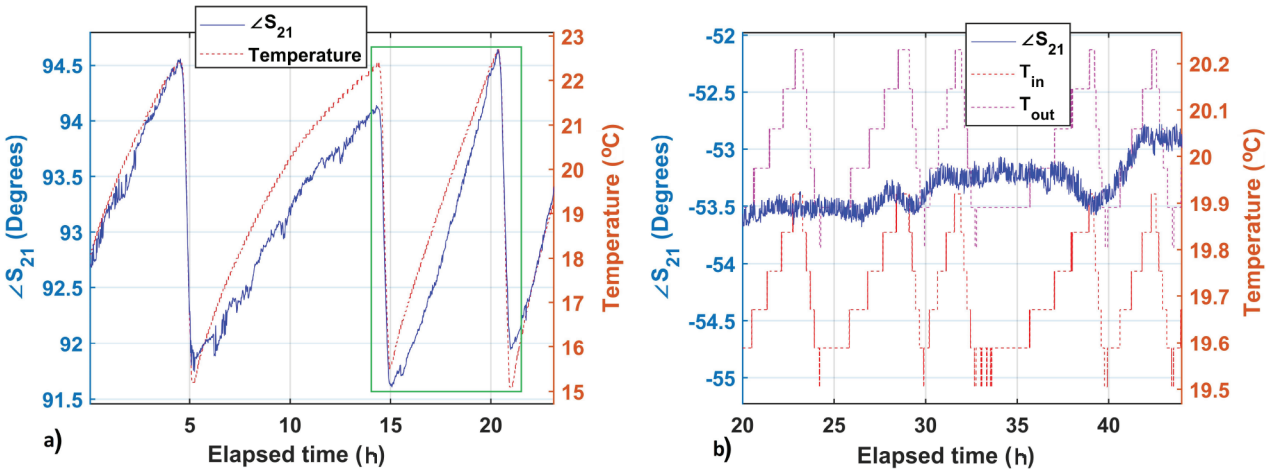

Figure 9. a) The phase of the transmission coefficient ($\angle S_{21}$) without phase shifter (zoomed portion from Figure 6d), b) the phase of the transmission coefficient ($\angle S_{21}$) (using phase shifter) in the improved setup.

degraded by the imbalance both in phase and amplitude at system level, in turn, affecting the basic parameters of output power such as efficiency and output reflection coefficient [19–22].

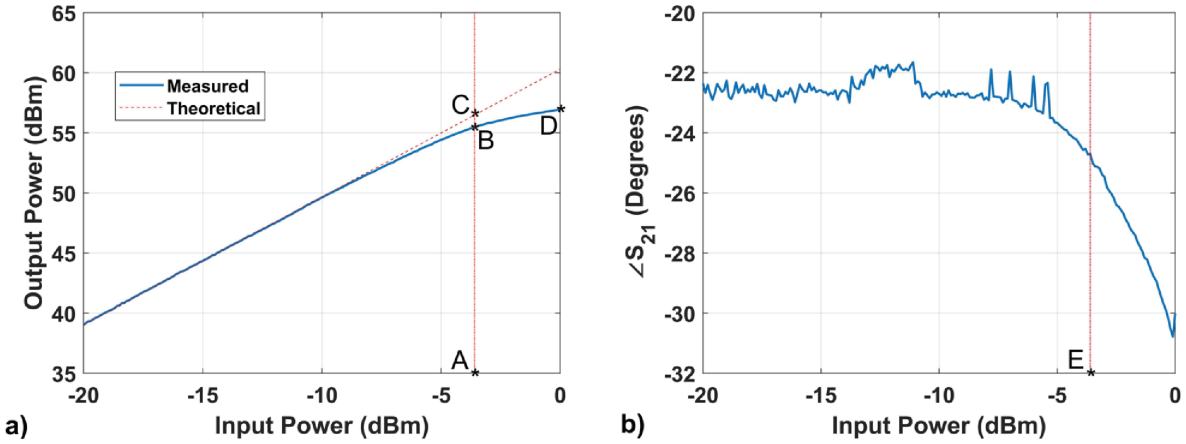

Figure 10. a) AM/PM characteristics of the amplifier under test [16]. a) Full scale output power variation: A* is to mark the input power level (–3.62 dBm) at which 1 dB compression occurs at the output power. Linear output power model assumes 56.47 dBm (444 W) as marked with C* while the actual output power which is marked by B* (at 1 dB compression) is 55.46 dBm (352 W). Maximum output power in the full range is 56.97 dBm (498 W), marked by D*, b) output phase variation as a function of excitation power of the amplifier, E* shows the same input power level (–3.62 dBm) at which 1 dB compression in output power occurs.

Variations in phase become more dominant in efficiency degradation in comparison to the effect of the variations in amplitude [19]. Besides many reasons like the amplitude/phase imbalance which occurs due to disturbances in the RF amplifier itself, mismatching/reflections at the bending and ending points of the high power RF cable, ambient conditions like water-cooling line temperature and pressure may cause degradation in efficiency.

In this study, amplitude variations and the extent of the phase imbalance of the 500 W solid state RF amplifier running at 1300 MHz are studied. For this purpose, based on the S-parameters model, measurements are performed to observe the amplitude as well as the phase of the transmitted power. The measurements are carried out by minimizing the phase variation with the proposed method which includes utilization of a manual phase shifter and a circulator in order to maintain the stability and to ensure lower reflection at the output of the power amplifier. The performance of the proposed method is tested by carrying out long term run measurements.

Achieving reduced phase variation in the transmitted RF power at high power levels is not a trivial process due to the electronics itself which also enforces incorporation of water cooling system to control temperature and pressure. Nevertheless, this reduction is of vital importance to increase the beam power interaction and to reduce the emittance growth and energy spread [4, 11] during beam transport.

The possibility that the phase variation arises from the amplifier is eliminated by examining geometrically derived stability parameters including Rollet's stability parameter. Based on the long duration S-parameter measurements, it is found that the system satisfies the unconditional stability conditions. As a result, it is verified that the phase alteration is not caused by the RF amplifier electronics itself. However, characterization of the performance of the high power RF amplifier from the perspective of water cooling system is poorly documented or not reported at all in the literature, to the best of authors' knowledge. In this sense, this study may serve as an initial guide for the researchers in the context of such high power RF applications.

Our measurements reveal the necessity of taking hard precautions towards the routine operation, by avoiding phase variation which disturbs the beam power interaction and limits the gain in FB. Thus, by

incorporating a manual phase shifter and a circulator in the system, the standard deviation of the ripple in the phase of transmission coefficient is reduced from 0.208 to 0.054. Additionally, the AM/PM characteristics of the RF amplifier validate the correction of the phase transmission of the output power with the improved circuit. Utilization of the phase shifter yields a strong correlation between the phase of the transmission coefficient and water temperature. The phase variation value of ~ 0.75 deg/°C which is encountered without the phase shifter is reduced to less than ~ 0.45 deg/°C by the use of phase shifter after the normalization with respect to temperature as described in Section 3. The phase correction is further accompanied with a reduction of the reflected power from 4.3 W ($\sim$ 36.33 dBm) to 3 mW ($\sim$ 4.7 dBm) at the output of the power amplifier. This study will be completed following the integration of the whole system including the main RF controller of the accelerator (LLRF), and testing the stability of the embedded system.

Acknowledgment

This work is supported by Presidency Strategy and Budget Directorate under Grant No: 2006K12-827 (2006K-120470). The authors would like to thank to the TARLA team for their supports in installing the experimental set-up.

References

[1] Aksoy A, Karslı Ö, Yavaş Ö. The Turkish accelerator complex ir fel project. Infrared Physics & Technology 2008; 51 (5): 378-381. doi: 10.1016/j.infrared.2007.12.027

[2] Yildiz H, Aksoy A, Arikan P. Effects of coherent synchrotron radiation in bunch compressor of tarla. Acta Physica Polonica A 2016; 130 (1): 214-216. doi: 10.12693/APhysPolA.130.214

[3] Zulick C, Hou B, Dollar F, Maksimchuk A, Nees J et al. High resolution bremsstrahlung and fast electron characterization in ultrafast intense laser–solid interactions. New Journal of Physics 2013; 15 (12): 123038. doi: 10.1088/1367-2630/15/12/123038

[4] Karsli O, Aksoy A, Kaya C, Koc B, Dogan M et al. High power rf operations studies at tarla facility. Canadian Journal of Physics 2019; 97 (11): 1171-1176. doi: 10.1139/cjp-2018-0778

[5] Aksoy A, Karsli O, Aydin A, Kaya C, Ketenoglu B et al. Current status of Turkish accelerator and radiation laboratory in Ankara: the tarla facility. Canadian Journal of Physics 2018; 96 (7): 837-842. doi: 10.1139/cjp-2017-0750

[6] Aune B, Bandelmann R, Bloess D, Bonin B, Bosotti A et al. Superconducting tesla cavities. Physical Review Special Topics-Accelerators and Beams 2000; 3 (9): 092001. doi: 10.1103/PhysRevSTAB.3.092001

[7] Gabriel F, Gippner P, Grosse E, Janssen D, Michel P et al. The rossendorf radiation source elbe and its fel projects. Nuclear Instruments and Methods in Physics Research Section B: Beam Interactions with Materials and Atoms 2000; 161: 1143-1147. doi: 10.1016/S0168-583X(99)00909-X

[8] Avino P, Petrucci A, Schulze D, Segebade C. Encyclopedia of Analytical Science. 3rd ed. Oxford, UK: Academic Press, 2019. doi: 10.1016/B978-0-12-409547-2.14370-7

[9] Branlard J, Ayvazyan G, Ayvazyan V, Grecki M, Hoffmann M et al. Mtca.4 llrf system for the European xfel. In: Proceedings of the 20th International Conference Mixed Design of Integrated Circuits and Systems - MIXDES 2013; New York, NY, USA; 2013. pp. 109-112.

[10] Schmidt C. Tarla llrf conceptual design report, Technical Report DESY. Hamburg, Germany: Deutsches Elektronen-Synchrotron (DESY), 2018.

[11] Karsli Ö, Colak E. Operation tests of the 260 MHz 1500 W solid state rf Amplifier at tarla facility. Communications Faculty of Sciences University of Ankara Series A2-A3 Physical Sciences and Engineering 2019; 61 (2): 181-196. doi: 10.33769/aupse.557951

[12] Liu X, Small J, Berdy D, Katehi LP, Chappell WJ et al. Impact of mechanical vibration on the performance of rf mems evanescent-mode tunable resonators. IEEE Microwave and Wireless Components Letters 2011; 21 (8): 406-408. doi: 10.1109/LMWC.2011.2160159

[13] Chen K, Liu X, Kovacs A, Chappell WJ, Peroulis D. Antibiased electrostatic rf mems varactors and tunable filters. IEEE Transactions on Microwave Theory and Techniques 2010; 58 (12): 3971-3981. doi: 10.1109/TMTT.2010.2088135

[14] Lombardi G, Neri B. Criteria for the evaluation of unconditional stability of microwave linear two-ports: a critical review and new proof. IEEE Transactions on Microwave Theory and Techniques 1999; 47 (6): 746-751. doi: 10.1109/22.769346

[15] Kassim S, Malek F. Microwave fet amplifier stability analysis using geometrically-derived stability factors. In: 2010 International Conference on Intelligent and Advanced Systems- ICIAS 2010; Kuala Lumpur, Malaysia; 2010. pp. 1-5. doi: 10.1109/ICIAS.2010.5716171

[16] Moulthrop AA, Clark CJ, Silva CP, Muha MS. A dynamic am/am and am/pm measurement technique. In: 1997 IEEE MTT-S International Microwave Symposium Digest; Colorado, USA; 1997. pp. 1455-1458. doi: 10.1109/MWSYM.1997.596604

[17] Nunes LC, Cabral PM, Pedro JC. A physical model of power amplifiers am/am and am/pm distortions and their internal relationship. In: 2013 IEEE MTT-S International Microwave Symposium Digest- (MTT) 2013; Seattle, WA, USA; 2013. pp. 1-4. doi:10.1109/MWSYM.2013.6697497.

[18] Wisell D. Measurement techniques for characterization of power amplifiers. Doctoral dissertation, KTH School of Electrical Engineering, Stockholm, Sweden, 2007.

[19] Jain A, Sharma DK, Gupta AK, Lad MR, Hannurkar PR et al. System efficiency analysis for high power solid state radio frequency transmitter. Review of Scientific Instruments 2014; 85 (2): 024707. doi: 10.1063/1.4866649

[20] Jain A, Hannurkar PR, Sharma DK, Gupta AK, Tiwari AK et al. Design and characterization of 50 kW solid-state rf amplifier. International Journal of Microwave and Wireless Technologies 2012; 4 (6): 595. doi: 10.1017/S175907871200061X

[21] Jain A, Sharma DK, Gupta AK, Hannurkar PR, Pathak SK. Compact solid state radio frequency amplifiers in kW regime for particle accelerator subsystems. Sadhana 2013; 38 (4): 667-678. doi: 10.1007/s12046-013-0154-0

[22] Jain A, Hannurkar PR, Pathak SK, Sharma DK, Gupta AK. Investigation of class J continuous mode for high-power solid-state rf amplifier. IET Microwaves, Antennas & Propagation 2013; 7 (8): 686-692. doi: 10.1049/iet-map.2012.0649